

Influence of burnout process on pore structure and burnout microstructure in BaTiO₃-based Y5V materials

Young-Kil Kim^a, Yeon-Gil Jung^a, Tae-Hyun Sung^b, Dae-Hawn Kim^c, Ungyu Paik^{c,*}

^a Department of Ceramic Science and Engineering, Changwon National University, Changwon, Kyungnam 641-773, South Korea

^b Advanced Technology Center, Korea Electric Power Research Institute, Daejeon 305-380, South Korea

^c Department of Ceramic Engineering, Hanyang University, Seoul 133-791, South Korea

Received 24 May 2002; received in revised form 6 April 2004; accepted 7 April 2004

Abstract

BaTiO₃-based multilayer ceramic capacitors (MLCCs) prepared by tape casting, showing Y5V characteristic, were fired with different burnout conditions. MLCCs show the delamination from the heating rate of 7 °C/min to 200 °C, and 6 °C/min to 250 and 300 °C in the ambient atmosphere, without the delamination in the reducing atmosphere. The pore size distribution of MLCCs becomes narrower with increases in the temperature and heating rate, showing larger pore size and mono-modal pore size distribution. The cumulative pore surface area shows minimum values at a higher temperature and faster heating rate in both atmospheres. However, MLCCs of the reducing atmosphere display a smaller cumulative pore surface area than that of the ambient atmosphere. The microstructure related to the burnout process is more dependent on atmosphere and temperature than heating rate. The possible causes for the burnout behavior and microstructure are also discussed.

© 2004 Elsevier B.V. All rights reserved.

Keywords: BaTiO₃; MLCCs; Burnout process; Pore; Microstructure

1. Introduction

The technology for the fabrication of multilayer ceramic capacitors (MLCCs) has progressed rapidly as results of down sizing and cost reduction. Recently, MLCCs with 3–4 μm and over 300 active layers are available, and with 2–3 μm and over 600 active layers have been developed. For this purpose, smaller size powder and cheaper base metal (e.g., nickel; Ni) need to be used as dielectric and electrode materials, respectively, which have to give more attention to burnout process for preventing the oxidation of base metal electrode and controlling the residual carbon from organic binders [1–3]. Also, a pore structure created by the burnout process and a relationship between the pore structure and the burnout process are to be important for the reliability and dielectric property of MLCCs.

There are many reports on the relationships between microstructure and dielectric properties, including the sintering of doped and undoped BaTiO₃ materials [4–7,10]. Few citations were even found where the effect of sintering atmosphere on dielectric properties was described [8,9],

which is related to X7R materials. The effect of burnout process on the pore structure and burnout microstructure of BaTiO₃-based Ni-MLCCs prepared by tape casting, showing Y5V dielectric characteristics, have not appeared in the literature.

In this study, influences of burnout atmosphere, temperature, and heating rate on pore size and distribution, pore structure, and burnout microstructure of MLCCs, showing Y5V characteristic, are investigated. The green MLCCs were fired under different conditions as functions of atmosphere, heating rate, and temperature in the burnout process. Also, the causes of delamination and pore formation during/after the burnout process are discussed with oxidation, pore size and distribution, cumulative pore surface, and microstructure in MLCCs.

2. Experimental procedure

2.1. Starting materials and preparation

The dielectric materials employed in this work are those with an Y5V characteristic whose main composition is Ba_{0.95}Ca_{0.05}Ti_{0.82}Zr_{0.18} (Kyorix Co., Japan) + various metal oxide additives (such as Y₂O₃, MnO₂, glass frit),

* Corresponding author. Tel.: +82 2 2290 0502; fax: +82 2 2281 0502.
E-mail address: upaik@hanyang.ac.kr (U. Paik).

totaling less than 1 wt.% of the formulation. Ni powder was used as an internal electrode.

The green MLCCs were prepared by the following procedure. The powders, organic binder (PVB series), dispersant (RE610, Toho Chemical, Japan), and plasticizer were mixed and dispersed in a nonaqueous media (mixture of toluene and ethanol; 80:20 ratio). The green sheet with a thickness of $\approx 9.5 \mu\text{m}$ was prepared by the slot-die method (on-roll method). After the electrode was printed on the green sheet, this was then laminated and isotropic pressed, and then cut into green chips. The final dimension of the green MLCCs after cutting is $\approx 4 \text{ mm} \times 2 \text{ mm} \times 2 \text{ mm}$ with 150 actives.

2.2. Characterization

Thermal behavior of the chips was analyzed by thermogravimetric analysis (TGA/DTA, SDT2960, TA Instrument,

USA) in the ambient and argon atmospheres. The burnout atmosphere was chosen as the ambient and reducing atmospheres controlling H_2 , Ar, O_2 and H_2O . Temperature and heating rate were selected as 200, 250 and 300°C , and controlled as $1\text{--}7^\circ\text{C}/\text{min}$ with 1°C interval, respectively, keeping holding time at the burnout temperature as 1 h.

Optical microscopy (EPIPHON, Nikon, Japan) was used for the investigation of the entire condition in MLCCs after the burnout process. Phase identification with the burnout atmosphere was performed by X-ray diffractometry (XRD, Rigaku Co., D/MAX-III, Japan). Pore size and distribution of MLCCs after the burnout process was measured by porosimetry (Autoscan-25, 60, Quantachrome Corp., Syosset, NY, USA), from which the cumulative pore surface area of MLCCs is compared [11–13]. The burnout microstructure in the fracture surface was observed by scanning electron microscopy (SEM, S2700, Hitachi, Japan).

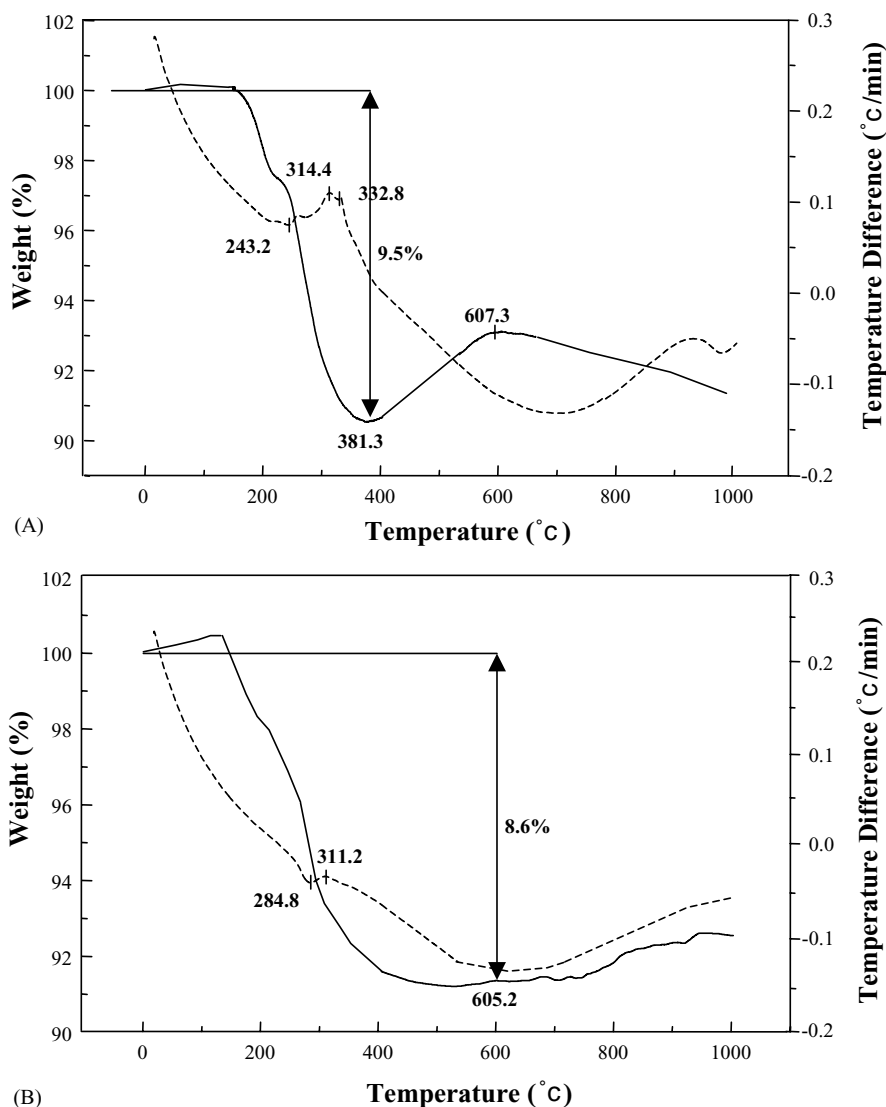


Fig. 1. TGA/DTA curves showing weight loss and gain in MLCCs during burnout process: (A) ambient atmospheres and (B) argon atmosphere. Solid curves indicate weight change (%) and dashed curves temperature difference ($^\circ\text{C}/\text{min}$)

3. Results and discussion

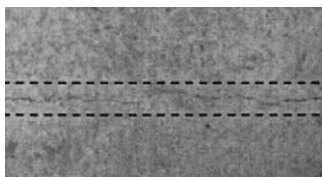
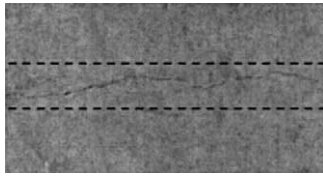
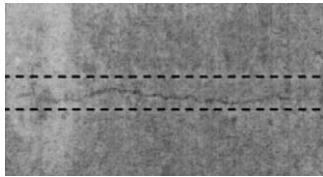
3.1. Thermal and burnout behavior

The burnout temperature to remove organic binder can be selected at 200, 250, and 300 °C from the result of Fig. 1. Also, the weight change and the exothermic peaks in TGA/DTA curve give the information for removal behavior of the binder and for oxidation of the electrode, respectively. In the ambient atmosphere (Fig. 1(A)), the sudden weight loss is observed from ≈200 to ≈380 °C, and then the gain to ≈607 °C is detected, considered as the removal of the binder and the oxidation of the electrode, respectively. The argon atmosphere (Fig. 1(B)) also shows the weight loss to ≈500 °C without the sudden weight change compared to the ambient atmosphere, and then the moderate increase. The exothermic peaks at 314 and 332 °C for the ambient, and 311 °C for the reducing are believed to be due to the oxidation of the electrode.

The weight gain in the argon atmosphere can be considered as the oxidation of the electrode due to the reaction between the activated electrode and the oxygen vaporized from the binder during the burnout process. The ambient atmosphere is effective in removing the binder at a lower temperature, but the oxidation of the electrode occurs from the temperature of ≈380 °C. In contrast, the burnout process in the argon atmosphere is less effective in removing the binder, but shows little adverse reaction at a higher temperature.

MLCCs after the burnout process display a delamination in the ambient atmosphere as shown in Table 1. The delamination is created in the middle of MLCCs from the heating rate of 7 °C/min to 200 °C, and 6 °C/min to 250 and 300 °C, showing sound condition below those heating rate conditions. Meanwhile, MLCCs prepared under the reducing at-

Table 1
Conditions of MLCCs after burnout process in ambient atmosphere as functions of heating rate and temperature

Atmosphere	
Condition	Ambient
200 °C, 7 °C/min	
250 °C, 6 °C/min	
300 °C, 6 °C/min	

mosphere (Ar/H₂ = 97/3) do not present any defects—such as the delamination and crack observed in the ambient atmosphere. These phenomena are strongly dependent on temperature and heating rate even though they will also be dependent on the composition of MLCCs, indicating that the higher burnout temperature needs the slower heating rate to prevent the delamination in MLCCs during the burnout process. In addition, because the delamination is created at the interface between electrode and active layers and at the

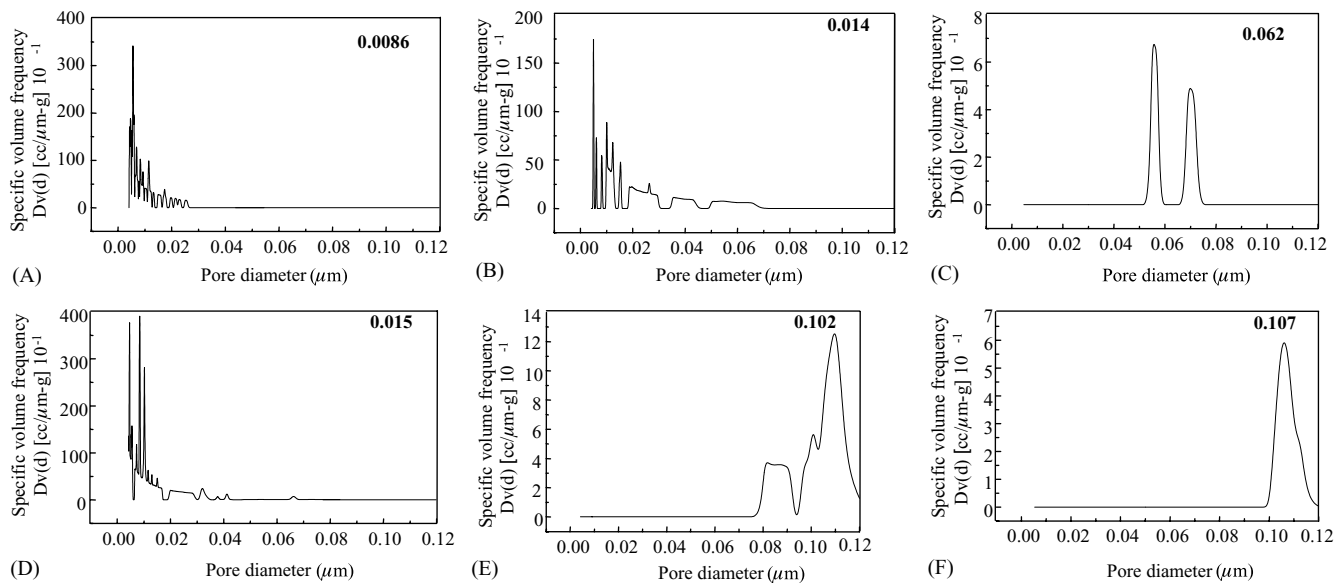


Fig. 2. Pore size and distributions of MLCCs after burnout process in ambient atmosphere: (A) 1 °C/min to 200 °C, (B) 1 °C/min to 250 °C, (C) 1 °C/min to 300 °C, (D) 3 °C/min to 250 °C, (E) 3 °C/min to 300 °C, and (F) 5 °C/min to 300 °C.

middle of MLCCs, the cause of the delamination can be considered as following [1,2,14–18]: (1) unbalance and insufficient pressing in lamination, (2) sudden oxidation of the electrode, and (3) combustion of the binder. Even though MLCCs prepared by the reducing atmosphere do not show the delamination on the outside, MLCCs with a faster heating rate in the burnout process will give some disadvantage to the firing process, resulting in firing defects such as inner cracks and residual stresses, etc. [8,19]. The effects of heating rate and temperature on microstructure and residual stresses developed in the end-products (MLCCs) are under-way and will be reported later.

3.2. Pore size distribution and pore structure

Fig. 2 shows the pore size distribution of MLCCs after the burnout process in the ambient atmosphere. The pore size distribution becomes narrower with an increase of temperature, showing bi-modal distribution in Fig. 2(C); even the mean pore size becomes larger. When the heating rate is increased, the bi-modal distribution becomes mono-modal. The mean pore size is also increased with an increase of the heating rate. Also, in the reducing atmosphere (Fig. 3), the pore size distribution becomes narrower with increases in the temperature and heating rate, showing mono-modal distribution at the heating rate of 5 °C/min to 300 °C. As a result, the burnout temperature and heating rate preferentially influence the pore size distribution and mean pore size, respectively.

The effects of temperature and heating rate on pore formation during the burnout process are more clearly observed in the cumulative pore surface as shown in Fig. 4. Even though the large pore is created in a higher temperature and faster heating rate as shown in Figs. 3 and 4, the cumulative pore surface area associated with the binder removal during the burnout process shows the minimum values in a higher temperature and faster heating rate, independent of the atmosphere. This means that the pore size increases and the pore volume decreases with increases in the temperature and heating rate. While the reducing atmosphere makes a smaller cumulative pore surface area than the ambient atmosphere after the burnout process, from which the burnout process can be allowed in the reducing atmosphere as the temperature of 300 °C and the heating rate of 5 °C/min. However, the other factors in the burnout process, such as the binder removal and burnout microstructure including residual carbon, have to be considered.

More specifically, the form of the pore channel (pore structure or pore shape) can be assumed with the hysteresis of intrusion/extrusion behavior in mercury porosimetry. Fig. 5 shows the comparison between intrusion/extrusion behaviors in MLCCs after the burnout process with the ambient and reducing atmospheres. The hysteresis behavior is dependent on the mean pore size and pore size distribution; even the absolute amounts of intrusion/extrusion are different. After the burnout process at 250 °C with 3 °C/min in the am-

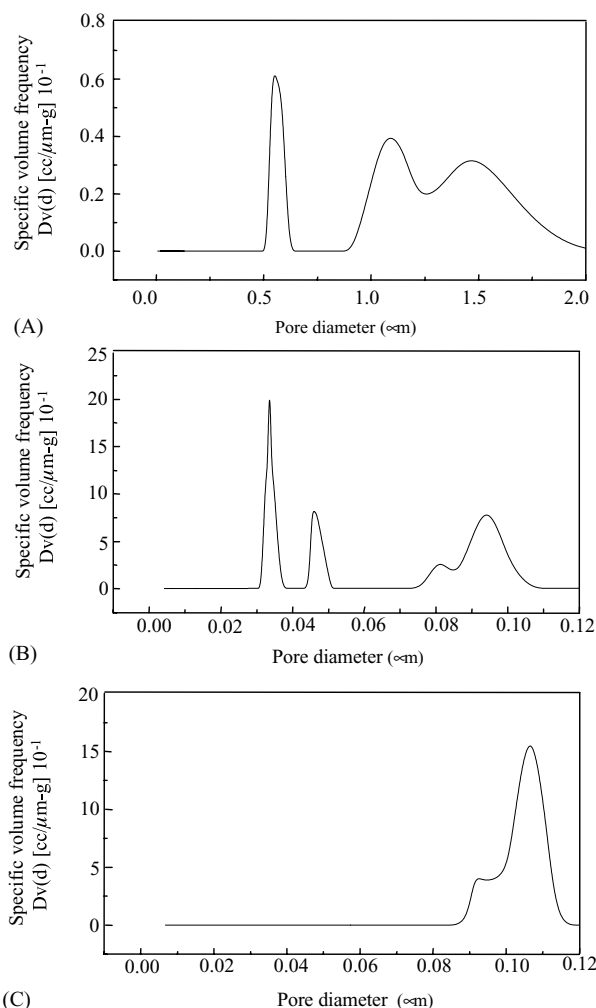


Fig. 3. Pore size and distributions of MLCCs after burnout process in reducing atmosphere: (A) 1 °C/min to 200 °C, (B) 3 °C/min to 250 °C, and (C) 5 °C/min to 300 °C.

bient atmosphere (Fig. 5(A)), almost 85% of the total mercury intruded remains in MLCCs. It is evident that mercury penetrated into the so-called ink-bottle pores, explained by the assumption of cylindrical pores in mercury porosimetry [14,15], will not leave these pores through the smaller pore entrance during extrusion. However, in the other hysteresis, the extrusion starts to take place at a much higher pressure. This means that the pore structures are open with each other and the pore shape is the ink-bottle pore with a broad neck. However, it can be argued that pore shape and structure will be determined by the mercury intrusion/extrusion behaviors (hysteresis behavior) because the amount of mercury retained by the sample will be influenced by a combination of at least two factors: the shape of the pores and the value of the contact angle [20].

Many reports have been offered to account for the experimental observation that mercury extrusion curves do not overlap intrusion curves [11,12,21–23]. Three explanations appear to be favored by different groups in the literature: (1)

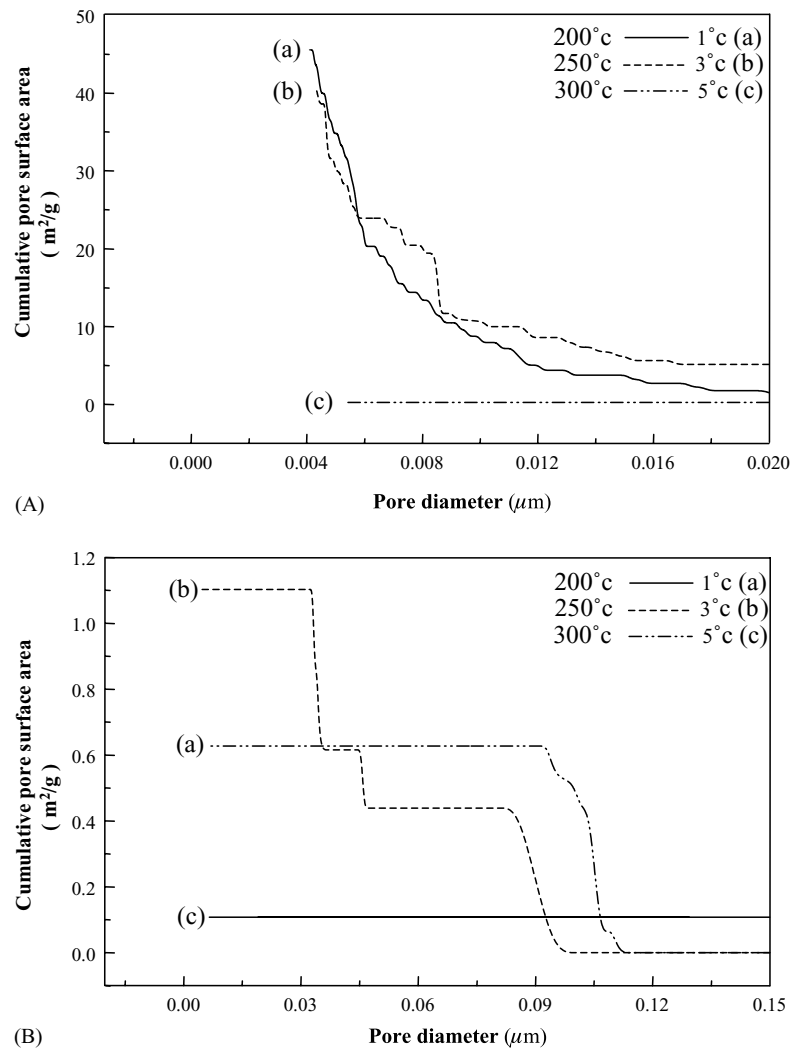


Fig. 4. Cumulative pore surface versus pore size of MLCCs after burnout process in both atmospheres: (A) ambient atmosphere with (a) 1°C/min to 200°C, (b) 3°C/min to 250°C, and (c) 5°C/min to 300°C; (B) reducing atmosphere with (a) 1°C/min to 200°C, (b) 3°C/min to 250°C, and (c) 5°C/min to 300°C.

the ink-bottle pore assumption [11,12], (2) network effects [21,22], and (3) the pore potential theory [23]. Usually, the pores of different size are assumed to be all of the same regular shape (e.g. cylinders or slits) and generally each pore is assumed to behave independently. In our system, the volume of mercury intruded is decreased with increases in temperature and heating rate. These results are well consistent with the observation of the pore size and distribution. Therefore, if the burnout process is performed at a lower temperature and slower heating rate, pore structure will show a narrower neck and larger inner volume than that of a higher temperature and faster heating rate.

3.3. Microstructure

The effects of heating rate, atmosphere, and temperature on the burnout microstructure can be clarified from Figs. 6 and 7. The ambient atmosphere is more effective in remov-

ing the binder than the reducing atmosphere, showing much of the binder between particles in the reducing atmosphere. While, in the ambient atmosphere, the particle surface is clearer compared to the reducing atmosphere as the evidence of combustion. However, the effect of the heating rate on the burnout microstructure is not observed in either atmosphere. As temperature is increased in the reducing atmosphere, the interface of particles is cleared (as shown in Fig. 7), showing the similar microstructure with the ambient atmosphere (Fig. 6(A) and (C)). Therefore, if the burnout process is performed in the ambient atmosphere, the binder can evaporate too quickly, resulting in the difference of pore structure within the chips. However, even in the reducing atmosphere, a faster heating rate can remove the binder suddenly, which can also affect the degree of densification in the sintered bodies.

As a result, the optimum burnout condition in this system is the temperature of 300°C, the heating rate of 1°C/min,

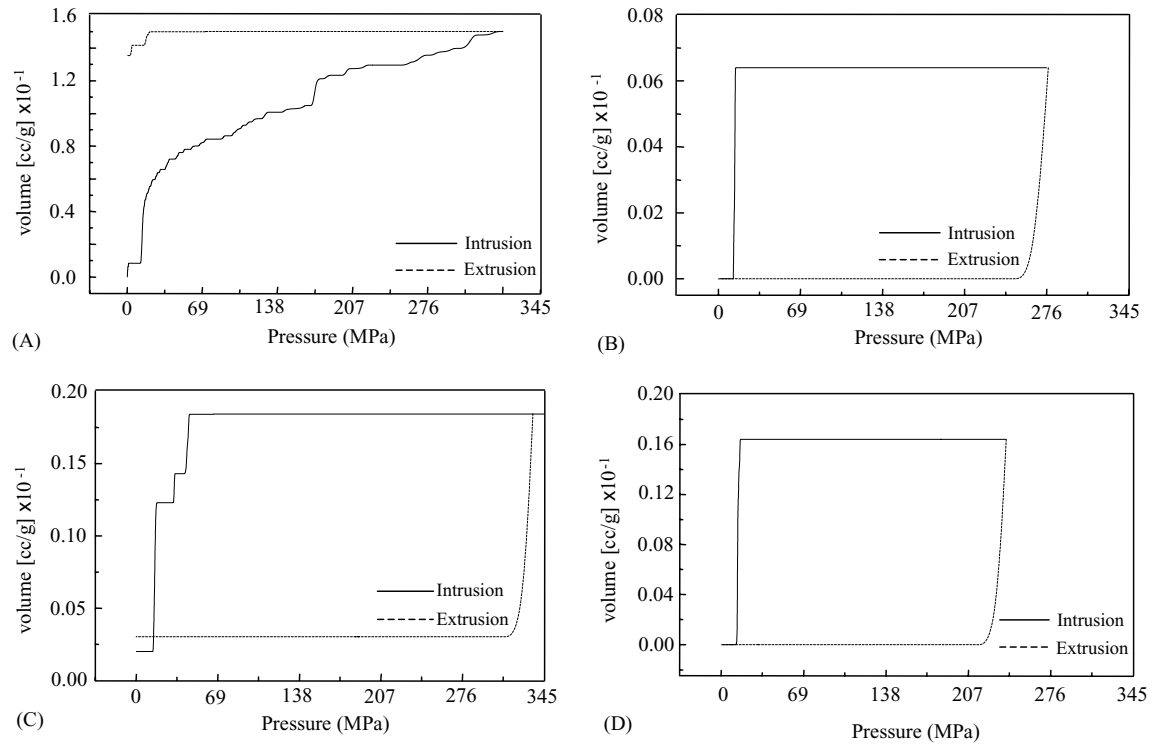


Fig. 5. Intrusion–extrusion curves of MLCCs after burnout process in both atmospheres: (A) 3 °C/min to 250 °C in ambient atmosphere, (B) 5 °C/min to 300 °C in ambient atmosphere, (C) 3 °C/min to 250 °C in reducing atmosphere, and (D) 5 °C/min to 300 °C in reducing atmosphere.

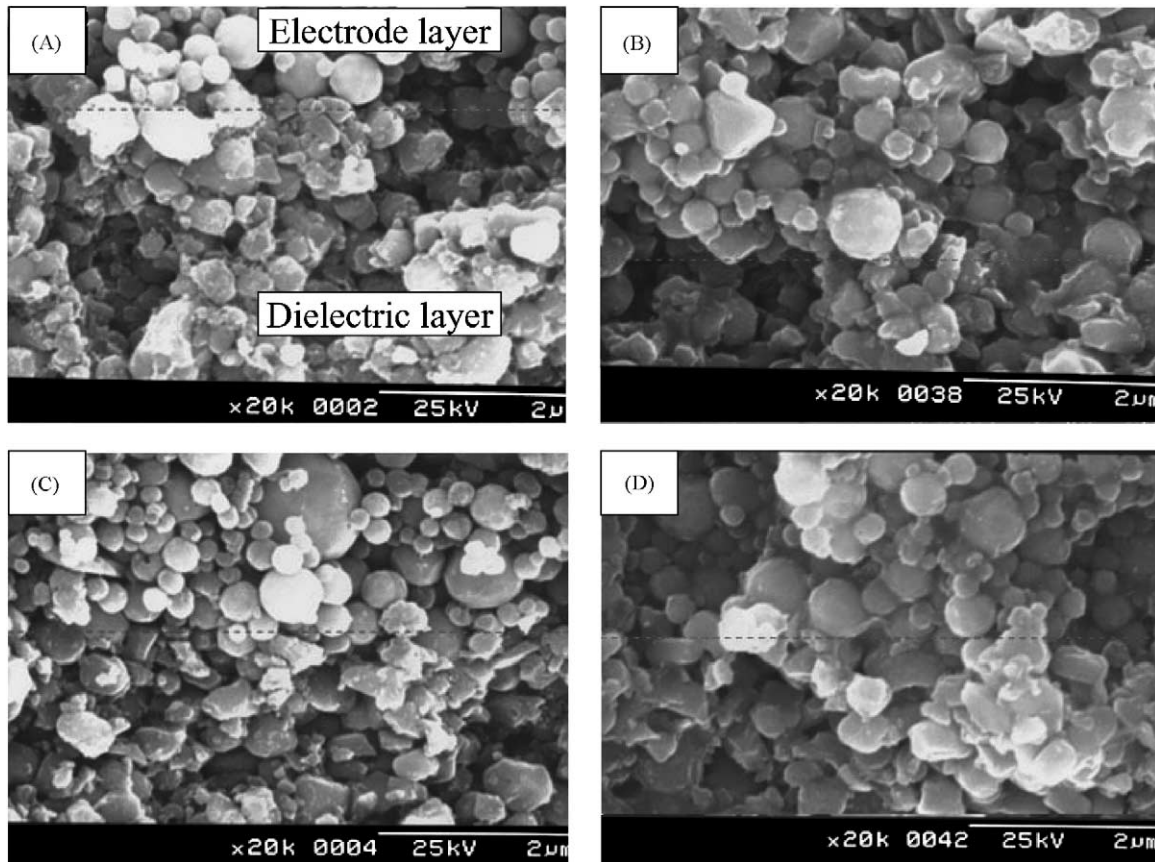


Fig. 6. Scanning electron micrographs of MLCCs after burnout process in both atmospheres: (A) 1 °C/min to 250 °C in ambient atmosphere, (B) 1 °C/min to 250 °C in reducing atmosphere, (C) 5 °C/min to 250 °C in ambient atmosphere, (D) 5 °C/min to 250 °C in reducing atmosphere.

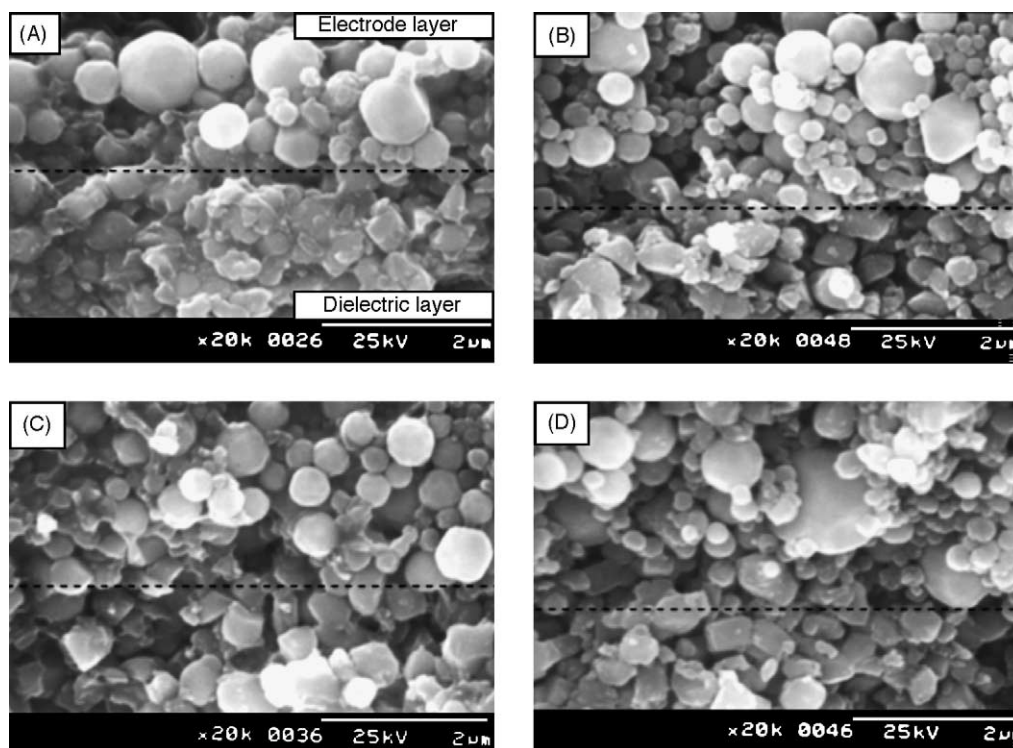


Fig. 7. Scanning electron micrographs of MLCCs after burnout process as functions of heating rate and temperature in reducing atmosphere: (A) 1 °C/min to 200 °C, (B) 1 °C/min to 300 °C, (C) 5 °C/min to 200 °C, and (D) 5 °C/min to 300 °C.

and the reducing atmosphere in the view of the cumulative pore surface area and microstructure related to the binder removal.

4. Conclusions

The burnout behavior of BaTiO₃-based Ni-MLCCs, showing Y5V characteristic, has been investigated by controlling atmosphere, temperature, and heating rate. The delamination in MLCCs is created at a faster heating rate in the ambient atmosphere, independent of temperature. However, MLCCs prepared under the reducing atmosphere (Ar/H₂ = 97/3) do not present any defects such as the delamination and cracks observed in the ambient atmosphere. Pore size is increased with increases in temperature and heating rate, resulting in a mono-modal distribution at a higher temperature and faster heating rate. The pore size distribution is affected by the heating rate in preference to temperature. On the other hand, MLCCs in the reducing atmosphere display a smaller cumulative pore area surface than those in the ambient atmosphere. Even the ambient atmosphere is more effective to remove the binder rather than the reducing atmosphere, which will give some disadvantage to the post process due to the heterogeneous pore structure and/or micro-cracking with the sudden removal of organic binder. The effects of the temperature and atmosphere on the burnout microstructure are superior to that of the heating rate.

Acknowledgements

This work was financially supported by the Korea Institute of Science and Technology Evaluation and Planning (KISTEP) through the 21 Century Frontier Projects.

References

- [1] T. Nomura, T. Kato, Y. Nagano, Proceedings of the Ninth US–Japan Seminar on Dielectric and Piezoelectric Ceramics, 1999, pp. 295–298.
- [2] T. Tsurumi, Y. Yamamoto, N. Ohashi, H. Chazono, Y. Inomata, H. Kishi, Proceedings of the 9th US–Japan Seminar on Dielectric and Piezoelectric Ceramics, 1999, p. 345.
- [3] Y. Sakabe, Dielectric materials for base-metal multilayer ceramic capacitors, *Am. Ceram. Soc. Bull.* 66 (1987) 1338–1341.
- [4] Y. Mizuno, Y. Okino, N. Kohzu, H. Chazono, H. Kishi, Influence of the microstructure evolution on electrical properties of multilayer capacitors with Ni electrode, *Jpn. J. Appl. Phys.* 37 (1998) 5227–5231.
- [5] Y. Okino, N. Kohzu, Y. Mizuno, M. Honda, H. Chazono, H. Kishi, Effects of the microstructure on dielectric properties for BaTiO₃-based MLC with Ni electrode, *Key Eng. Mater.* 157 (1999) 9–15.
- [6] H. Chazono, Y. Okino, N. Kohzu, H. Kishi, Effect of Sm and Ho addition on the microstructure and electrical properties in MLCC with Ni internal electrode, *Ceram. Trans.* 97 (1999) 53–64.
- [7] Y. Mizuno, T. Hagiwara, H. Chazono, H. Kishi, Effect of milling process on core-shell microstructure and electrical properties for BaTiO₃-based Ni-MLCC, *J. Euro. Ceram. Soc.* 21 (2001) 1649–1652.
- [8] D.F.K. Hennings, Dielectric materials for sintering in reducing atmospheres, *J. Euro. Ceram. Soc.* 21 (2001) 1637–1642.

- [9] N. Halder, D. Chattopadhyay, A.D. Sharma, D. Saha, A. Sen, H.S. Maiti, Effect of sintering atmosphere on the dielectric properties of barium titanate based capacitors, *Mater. Res. Bull.* 36 (1991) 905–913.
- [10] Y. Park, Y.H. Kim, H.G. Kim, The effect of grain size on dielectric behavior of BaTiO₃-based X7R materials, *Mater. Lett.* 28 (1996) 101–106.
- [11] S. Westermarck, A.M. Juppo, L. Kervinen, J. Yliruusi, Pore structure and surface area of mannitol powder, granules and tablets determined with mercury porosimetry and nitrogen adsorption, *Euro. J. Pharm. Biopharm.* 46 (1998) 61–68.
- [12] N. Das, H.S. Maiti, Formation of pore structure in tape-cast alumina membranes—effects of binder content and firing temperature, *J. Membr. Sci.* 140 (1998) 205–212.
- [13] C. Alie, R. Pirard, J.P. Pirard, Mercury porosimetry applied to porous silica materials: successive buckling and intrusion mechanisms, *Coll. Surf. A* 187–188 (2001) 367–374.
- [14] H. Chazono, Y. Inomata, N. Kohzu, H. Kishi, in: N. Mizutani, K. Shinozaki, N. Kamhara, T. Kimura (Eds.), *Electroceramics in Japan II*, Trans. Tech. Publications Ltd., CSJ Series, vol. 5, 1999.
- [15] H. Chazono, Y. Inomata, N. Kohzu, H. Kishi, in: N. Mizutani, K. Shinozaki, N. Kamhara, T. Kimura (Eds.), *Electroceramics in Japan III*, Trans. Tech. Publications Ltd., CSJ Series, vol. 6, 1999.
- [16] S. Masia, P. Calvert, W.E. Rhine, H.K. Bowen, Effect of oxides on binder burnout during ceramics processing, *J. Mater. Sci.* 24 (1989) 1907–1912.
- [17] M.J. Cima, M. Dudziak, J.A. Lewis, Observation of poly(vinylbutyral)-dibutyl phthalate binder capillary migration, *J. Am. Ceram. Soc.* 24 (1989) 1087–1090.
- [18] K. Hirakata, S. Sato, F. Uchikoba, Y. Kosaka, K. Sawamura, Multilayer capacitors with copper inner electrodes, *Ferroelectrics* 133 (1992) 139–144.
- [19] G. de With, Structural integrity of ceramic multilayer capacitor materials and ceramic multilayer capacitors, *J. Euro. Ceram. Soc.* 12 (1993) 323–336.
- [20] L. Moscou, S. Lub, Practical use of mercury porosimetry in the study of porous solids, *Power Tech.* 29 (1981) 45–52.
- [21] F.A.L. Dullien, *Porous Media: Fluid Transport and Pore Structure*, second ed., Academic Press, New York, 1992.
- [22] G.P. Matthews, C.J. Ridgway, M.C. Spssearing, Void space modeling of mercury intrusion hysteresis in sandstone, *J. Coll. Interface Sci.* 171 (1995) 8–27.
- [23] S. Lowell, J.E. Shields, *Powder Surface Area and Porosity*, third ed., Chapman Hall, New York, 1991.